Hindawi
International Journal of Analytical Chemistry
Volume 2018, Article ID 4371064, 10 pages
https://doi.org/10.1155/2018/4371064

Research Article

Structural Study of Europium Doped Gadolinium Polyphosphates $LiGd(PO_3)_4$ and Its Effect on Their Spectroscopic, Thermal, Magnetic, and Optical Properties

Saoussen Hammami,[1] **Nassira Chniba Boudjada**,[2] **and Adel Megriche**[1]

[1] *Université de Tunis El Manar, Faculté des Sciences de Tunis, UR11ES18 Unité de recherche de Chimie Minérale Appliquée. Campus Universitaire Farhat Hached, 2092 Manar 1. Tunis, Tunisia*
[2] *Institut Néel, BP 166, 38042 Grenoble Cedex 9, France*

Correspondence should be addressed to Saoussen Hammami; sosanehammami@gmail.com

Received 13 December 2017; Accepted 29 March 2018; Published 19 June 2018

Academic Editor: Adil Denizli

Alkali metal-rare earth polyphosphates $LiGd_{(1-x)}Eu_x(PO_3)_4$ (LGP:Eu^{3+}) (where x= 0, 0.02 and 0.04) were synthesized by solid-state reaction. The Rietveld refinement showed the following cell parameters: I 2/a space group, a=9.635(3) Å, b=7.035(3) Å, c=13.191(3) Å, β=90.082°, V= 894.214Å3, and Z=4. The similarity between R_F=4.21% and R_B=4.31% indicated that the realized refinement is reliable. The crystal structure consists of infinite zig-zag chains of $(PO_4)^{3-}$ tetrahedra, linked by bridging oxygen. The acyclic structure of polyphosphates is confirmed by infrared and Raman (IR) spectroscopies. A good thermal stability up to 940°C and paramagnetic behavior of these compounds were also proved by thermal analyses and magnetic susceptibility measurements, respectively. Excitation spectra revealed the charge transfer phenomenon between O^{2-} and Eu^{3+} (CTB), the energy transfer from Gd^{3+} to Eu^{3+}, and the intrinsic 4f-4f transitions of Eu^{3+} where the electronic transitions were also identified. Moreover, LGP:Eu^{3+} can emit intense reddish orange light under excitation at 394 nm. The strongest tow at 578 and 601 nm can be attributed to the transitions from excited state $^5D_0$ to ground states $^7F_1$ and $^7F_2$, respectively.

1. Introduction

Condensed alkali metal-rare earth polyphosphates, with the general formula $M^IRE^{III}(PO_3)_4$ (where M^I= are alkali metal and RE^{III}= are rare earth ions), have been extensively investigated thanks to their structural diversity [1–4] and their interesting magnetic [5], optic [6], and electric [7] proprieties. These polyphosphates are generally stable in normal conditions of temperature and humidity [8], which makes them useful for industrial applications. For example, Yamada et al. have used the $LiNd(PO_3)_4$ polyphosphate as a solid-state laser material [9, 10]. However, Z. Mua et al. have used $LiEu(PO_3)_4$ compound for white light-emitting diodes [11]. They are also used as promising scintillation material such as the Ce^{3+} doped $MGd(PO_3)_4$ compound [12].

In order to enhance the optical properties of polyphosphates, researches were oriented to doping them with metal-rare earths. In recent years, a great interest was accorded to europium earth-rare due to its outstanding photoluminescence feature [13–19]. In fact, the presence of well-defined energy levels in europium allows the emission of monochromatic and coherent radiations in solid laser.

The Gd–Eu couple is well known for its efficient conversion of the absorbed high-energy photons into two visible ones [20–24]. This phenomenon may be followed by a sequence of two steps of energies transfer. The first step is the transition $^6G_J \rightarrow {}^6P_J$ of Gd^{3+}, involving the $^5D_0 \rightarrow {}^7F_1$ transition of the Eu^{3+} ion. The one red photon related to the Eu^{3+} $^5D_0 \rightarrow {}^7F_J$ transition is created. In the second step, the energy of Gd^{3+} is related to $^6P_{7/2} \rightarrow {}^8S$ transition which is transported over the Gd^{3+} sublattice and then transferred to

another Eu^{3+} ion. This phenomenon leads to ^5D_J emission (J = 0, 1, 2, or 3) [25].

This work describes the synthesis of $LiGd_{(1-x)}Eu_x(PO_3)_4$ polyphosphate, doped with different low percentages of europium (2 and 4%). The structural study of all obtained compounds is carried out with XRD diffraction. The infrared and Raman spectroscopies and magnetic and thermal analyses were recorded at room temperature. Moreover, the optical study through excitation and emission of Eu^{3+} ions spectra was also undertaken.

2. Experimental

The condensed phosphates $LiGd_{(1-x)}Eu_x(PO_3)_4$ (where x= 0, 0.02 and 0.04) were synthesized by solid-state reaction (methods of Hammami et al. 2017) [26]. A mixture of the reagents, Li_2CO_3, Gd_2O_3, Eu_2O_3, and $NH_4H_2PO_4$, was prepared with the molar ratio (2.1:1:8) of Li:Gd:P, respectively. First, the raw materials were grounding in an agate mortar for one hour at least to homogenize the solid phase and improve the interatomic diffusion. Second, the mixture was introduced into the oven and submitted to the following thermal program. The first level was at 430°C to eliminate H_2O, NH_3, and CO_2, the second one was at 730°C to get $LiGd_{(1-x)}Eu_x(PO_3)_4$ pure phase. Then, the obtained products were cooled with the rate of 2°C/min to ensure a better crystallinity. Finally, the synthesized polyphosphates were washed with boiling water and nitric acid solution (1mol/L) to eliminate the residual raw materials from the final product.

The proposed chemical reaction for polyphosphate synthesis is

$$8NH_4H_2PO_4 + (1\text{-}x)\,Gd_2O_3 + xEu_2O_3 + Li_2CO_3 \longrightarrow 2\,LiGd_{(1-x)}Eu_x(PO_3)_4 + 8NH_3\uparrow + 12H_2O + CO_2\uparrow \quad (1)$$

Samples were characterized using an INEL XRG 3000 (D5000T) diffractometer with monochromatic Cu K_α radiation. The diffraction pattern was recorded under 300K over the angular range 10-90° (2θ). The luminescence spectra were performed under ambient atmosphere via Xenius (the fluorescence Genius) spectrophotometer, at 591nm and 394nm for excitation and emission, respectively. The infrared spectra were recorded in the range of 250–1500 cm^{-1} with a Thermo Scientific Nicolet N10 MX using sample dispersed in KBr pellets. Raman analysis was carried out at room temperature, with 514.5 nm radiation from an argon ion laser as the excitation beam. A microscope allowed a selection of high optical quality regions in the crystalline sample. Thermal stability of Eu^{3+} doped LGP was measured with differential thermal analysis SETARAM TAG 16 operating from room temperature up to 1000°C with heating rate of 5°C min^{-1}. Magnetic measurements were carried out using Quantum Design MPMSXL magnetometer with detection SQUID (at institute NEEL France).

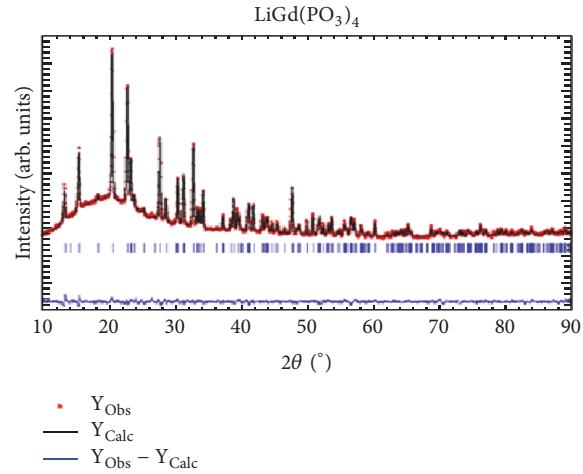

Figure 1: The Rietveld analysis of X-ray diffraction patterns for $LiGd(PO_3)_4$.

3. Results and Discussion

3.1. Rietveld Refinement Data Analyses. The Rietveld refinement of X-ray diffraction patterns of synthesized $LiGd(PO_3)_4$ samples is shown in Figure 1. The graph presents the experimental and the calculated data as well as the difference between them. As it is shown, the presence of only single phase was checked by Rietveld fitting quality through the reliability R factors: R_{exp}, R_{brag}, profile R_p, and weighted profile R_{wp}, which should be less than 10%. The final R factors, atomic coordinates, site occupancy, thermal displacement parameters, and their estimated standard deviations in parentheses for LGP are shown in Table 1. Interatomic bond distances and angles are given in Table 2. The new lattice parameters, derived from the Rietveld refinement, are a=9.635(3) Å, b= 7.035(3) Å, c= 13.191(3) Å, and β= 90.082° and with monoclinic space group I 2/a.

The LGP structure can be simply described as three-dimensional framework of GdO_8 polyhedra linked to $(PO_4)^{3-}$ rings by Gd-O-P bridges. This framework delimits interesting tunnels with Li^+ ions which are bonded to four oxygen atoms (LiO_4). Each LiO_4 tetrahedron shares all four O atoms with two LaO_8 polyhedra and four different PO_4 tetrahedra. A view of this structure projected along the b axis is shown in Figure 2.

3.2. X-Ray Powder Diffraction. X-ray diffraction patterns of $LiGd_{(1-x)}Eu_x(PO_3)_4$ (where x= 0, 0.02 and 0.04) are shown in Figure 3. The obtained crystalline phases are isotypes of the mother-phase $LiGd(PO_3)_4$ [27]. Mainly, it is shown that XR diffraction peaks of studied solids, with different percentages of europium, are described in a cell with a super space group I 2/a instead of C 2/c usually used in crystallographic data of the old LGP. The same XRD pattern is obtained for almost of synthesized compounds, even at high Eu^{3+} concentrations. However, a shift of the diffraction peaks to the lower 2θ is observed. This shift can be explained by Bragg's theory "$\mathbf{n\lambda = 2d_{hkl}\sin\theta}$" (where λ is the X-ray wavelength (Cu K_α

Table 1: Refined structure parameters from powder X-ray Rietveld analysis for $LiGd(PO_3)_4$ in space group I 2/a.

Atom	Wyck	x	y	z	B	Occ
Gd	4e	0.75000	0.2982(3)	0.00000	1.35(8)	0.50
Li	4e	0.75000	0.79603(4)	0.00000	1.88(16)	0.50
P1	8f	0.48189(3)	0.06204(4)	0.143135(20)	1.88(16)	1.00
P2	8f	0.54601(3)	0.66399(4)	0.15354(2)	1.88(16)	1.00
OL12	8f	0.5665(6)	0.87995(6)	0.1598(14)	2.7(2)	1.00
OL21	8f	0.4057(4)	0.0815(16)	0.2447(3)	2.7(2)	1.00
OE21	8f	0.6520(11)	0.59342(6)	0.0754(8)	2.7(2)	1.00
OE11	8f	0.5743(13)	0.2282(14)	0.1098(11)	2.7(2)	1.00
OE22	8f	0.3953(6)	0.626(2)	0.1220(12)	2.7(2)	1.00
OE12	8f	0.3696(12)	0.0106(3)	0.0652(10)	2.7(2)	1.00
	R_p = 1.237	R_{wp}= 1.598	R_{exp} = 1.134	R_{Bragg}= 4.301	χ^2= 2	

Table 2: Atomic distances(Å) and angles in $LiGd(PO_3)_4$ with standard deviations in parentheses.

Tetrahedra	**aroundP1**				
P1-OL12	1.534(4)	OL12 -OL21	2.381(12)	$OL12^{i}$ —P1—OE11	111.61(38)
P1-OL21	1.535(4)	OL12 -OE21	2.446(11)	$OL12^{i}$ —P1—OL21	101.76(23)
P1-OE11	1.534(11)	OL12 -OL21	2.463(14)	$OL12^{i}$ —P1—OE12	105.86(29)
P1-OE12	1.535(12)	OL12 -OE11	2.538(11)	OL21—P1—OE11	117.46(53)
		OL12 -OE22	2.482(12)	OL21—P1—OE12	105.55(40)
		OL12 -OE12	2.448(15)	OE12—P1—OE11	113.37(47)
Tetrahedra	**around P2**				
P2 -OL12	1.5343(13)	OE22 -OL12	2.482(12)	OE22—P2—OE21	113.09(39)
P2 -OL21	1.534(6)	OE22 -OL21	2.619(12)	OE22—P2—OL12	108.04(41)
P2 -OE21	1.535(10)	OE22 -OE21	2.560	$OE22—P2—OL21^{vi}$	117.27(36)
P2 -OE22	1.533(7)	OL21 -OL12	2.381(12)	OE21—P2—OL12	105.66(4)
		OL21 -OL12	2.440(11)	$OE21—P2—OL21^{vi}$	105.25(16)
		OE21 -OE22	2.560(13)	$OL12—P2—OL21^{vi}$	106.79(38)
Polyhedra	**around Gd**	**Tetrahedra around Li**			
Gd -OE21	2.489(6)	Li -OE21		$Gd -Gd^{iv}$	5.592(2)
Gd -OE21	2.489(6)	Li -OE21		$Li -Gd^{ii}$	3.533(2)
Gd -OE11	2.283(13)	Li -OE12		$Li -Li^{v}$	5.068(0)
Gd -OE11	2.283(13)	Li -OE12		P1 - P2	2.8710(4)
Gd-OE22	2.197(13)			P2 -P1	2.7897(4)
Gd-OE22	2.197(13)			$Gd -P1^{iii}$	6.256(2)
Gd-OE12	2.605(7)				
Gd -OE12	2.605(7)				
Symmetry code	i: x,1+y,z	ii:x,1+y,z iii:1.5-x,1+y,-z		iv:2-x,1-y,-z v:2-x,2-y,-z	vi:1-x,0.5+y,0.5-z

=1.5406Å), θ is diffraction angle, and d is interplanar distance of corresponding diffraction peaks). Therefore, λ is constant; it can be concluded that this shift is due to the increase of interplanar distance "d". Considering the characteristics of Gd and Eu (ionic radius of Gd^{+3}: 1.05 Å, Eu^{+3}: 1.07 Å and atomic volume Gd: 19.9 cm^3/mol, Eu: 28.9 cm^3/mol), this phenomenon can be attributed to the distortion of the tetrahedra of polyphosphates upon europium insertion [28].

The crystallite size of obtained polyphosphates is calculated using Sherrer's equation below [29] and values are summarized in Table 3. Results show that the range of calculated crystallite size is between 42.49 and 42.79 nm, which prove that the synthesized compounds are nanometric.

$$\text{Sherre'r equation: } D = \frac{0.9\lambda}{\beta \cos\theta} \tag{2}$$

Table 3: The size of the crystallite according to percentage of europium.

Percentages (%)	FWHM	Position(2θ)	D(nm)
0	0.189	20.630	42.49
2	0.189	20.628	42.79
4	0.189	20.621	42.79

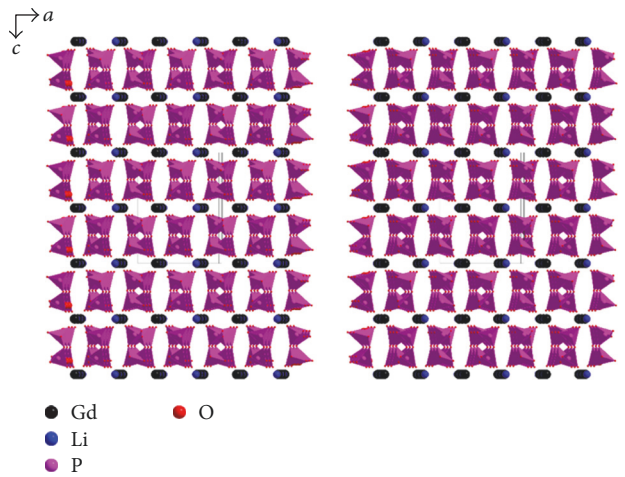

Figure 2: The structural arrangement of the $LiGd(PO_3)_4$ viewed in the (0 1 0) plane.

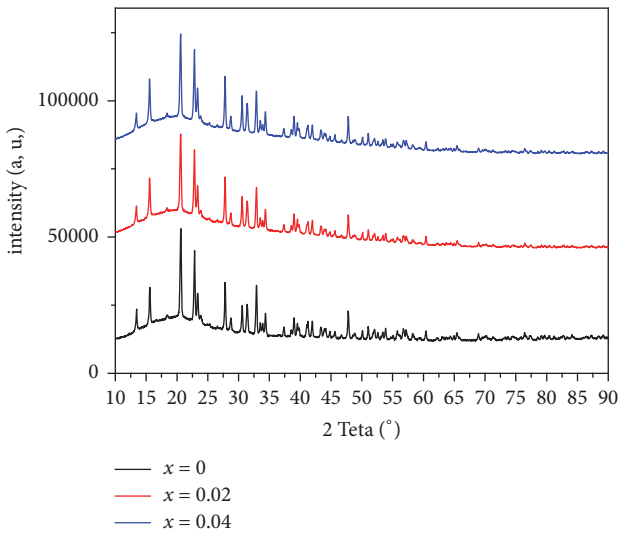

Figure 3: XRD patterns of $LiGd_{(1-x)}Eu_x(PO_3)_4$ (x=0, 0.02 and 0.04).

where λ is the X-ray wavelength (Cu K_α =1.5406Å), θ is the Bragg diffraction angle, and βe is the full width at half - maximum (FWHM) in radian of the main peak of each XRD pattern.

3.3. Infrared and Raman Spectroscopy Investigations

3.3.1. Infrared. Figure 4 shows the IR spectra of all studied compounds. The comparison of spectra (Figure 4) and those obtained in previous works in literature for condensed

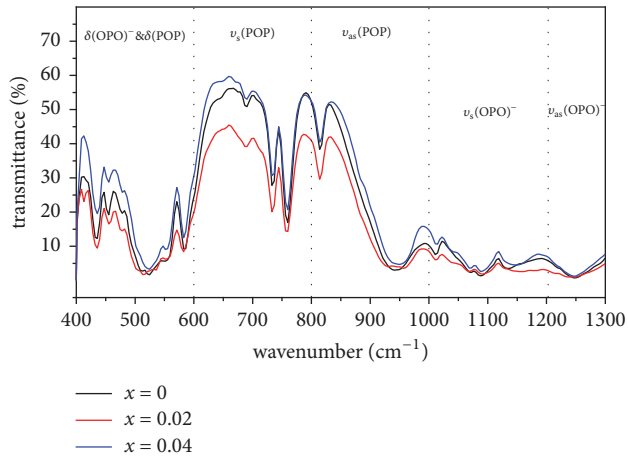

Figure 4: IR spectra of $LiGd_{(1-x)}Eu_x(PO_3)_4$ (x=0, 0.02 and 0.04).

polyphosphates [30, 31] proves that positions of infrared absorption bands are characteristic of phosphates with chain structures.

IR bands attribution is carried out based on $(O\text{-}P\text{-}O)^-$ groups and P-O-P bridges vibrations [32, 33]. The IR absorption spectra show the presence of two bands around 1249 cm^{-1} which are assigned to the asymmetric stretching vibration (υ_{as}) of O-P-O. The weak band observed between 1071 and 1136 cm^{-1} is attributed to the symmetric stretching vibration υ_s of O-P-O. The large and intense band around 944 cm^{-1} is assigned to the asymmetric vibration υ_{as} of P-O-P. We can also attribute the few bands at 689-818 cm^{-1} to the symmetric vibration υ_s (P-O-P). At low frequencies region, below 600 cm^{-1}, it is very difficult to distinguish the symmetric and antisymmetric bending modes of the (O-P-O) and (P-O-P) groups. The frequencies of the corresponding bands are given in Table 4.

The major difference between the IR spectra of cyclic polyphosphate and polyphosphate is the absence of vibration bands between 750 and 1000 cm^{-1}. In this range, IR spectroscopy confirms the structure as long as polyphosphates chains.

3.3.2. Raman. The Raman spectra of $LiGd_{(1-x)}Eu_x(PO_3)_4$ (where x= 0, 0.02 and 0.04) at room temperature are shown in Figure 5. These spectra show the presence of many bands; the first intense band at 1178 cm^{-1} and the second at 700 cm^{-1} are assigned to antisymmetric stretching vibration mode υ_{as} (O-P-O) and symmetric stretching vibrations mode υ_s (P-O-P), respectively. The υ_{as} (P-O-P) asymmetric and υ_s (O-P-O) symmetric stretching vibration modes, respectively, appear in the 1000-1100 cm^{-1} and 1212-1296 cm^{-1} ranges. The bands under 599 cm^{-1} are attributed to the symmetric and the asymmetric bending vibrations (δ_{as} and δ_s) of $(O\text{-}P\text{-}O)^-$ and (P-O-P). The intense symmetric stretching vibrations bands around 700 and 1178 cm^{-1} are characteristic of phosphoric anions $(PO_3)_4^{4-}$ [34].

Distinguishing characteristic cyclotetraphosphates and polyphosphates compounds exit also in the Raman spectrum.

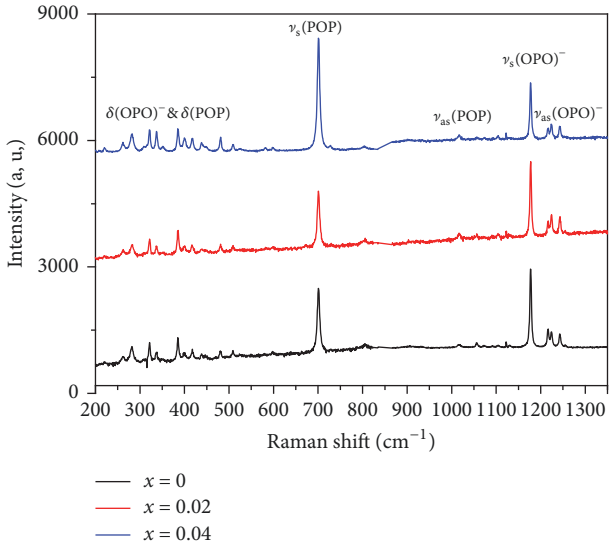

Figure 5: Raman spectra of $LiGd(PO_3)_4$ (x=0, 0.02 and 0.04) at 300 K.

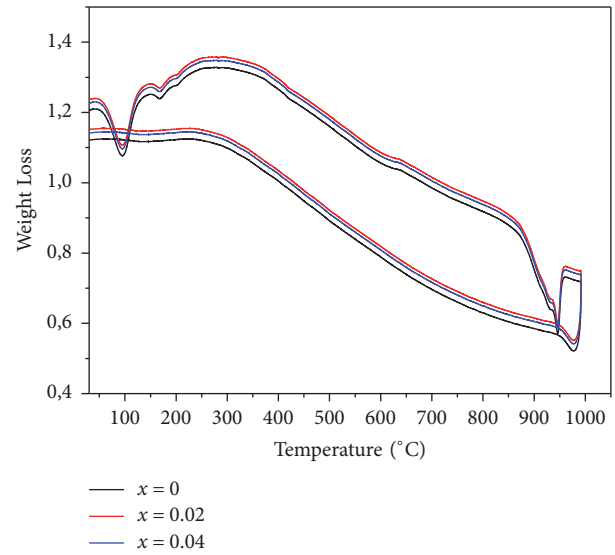

Figure 6: DTA of $LiGd_{(1-x)}Eu_x(PO_3)_4$ (x=0, 0.02 and 0.04).

Table 4: Attributions of main IR bands (cm^{-1}) of $LiGd_{(1-x)}Eu_x(PO_3)_4$ samples.

Assignment	x=0	x=0.02	x= 0.04
υ_{as} OPO	1257	1241	1250
	1137	1127	1149
υ_s OPO	1089	1089	109
υ_{as} POP	1014	1014	1014
	944	944	947
υ_s POP	689	689	689
	736	736	736
	761	758	761
	818	818	818
δPOP	437-	437	437
δPOP	456	456	457
	519	519	521
	586	585	585

The symmetric stretching vibration of the P-O-P (υ_s (P-O-P)) has a single band at 700 cm^{-1}. This is the strongest of all the Raman vibration bands. That is because of the monoclinic symmetry of LGP doped Eu and the different positions of the lanthanide and alkali ions. The results of Raman spectroscopy can identify the structure of alkali metal lanthanide polyphosphates.

3.4. DTA (Differential Thermal Analysis). The thermal stability of lithium polyphosphate is investigated using DTA. The curves of the Eu: $LiGd(PO_3)_4$ crystal are given in Figure 6. It is clearly observed that the curves present the same shape (evolution). Indeed, a single sharp endothermic peak is observed between 900 and 1000°C for all samples, which exhibits the characteristics of a first-order phase transition. This signal can be attributed to the decomposition of polyphosphates to $GdPO_4$. The stability of lithium gadolinium polyphosphates

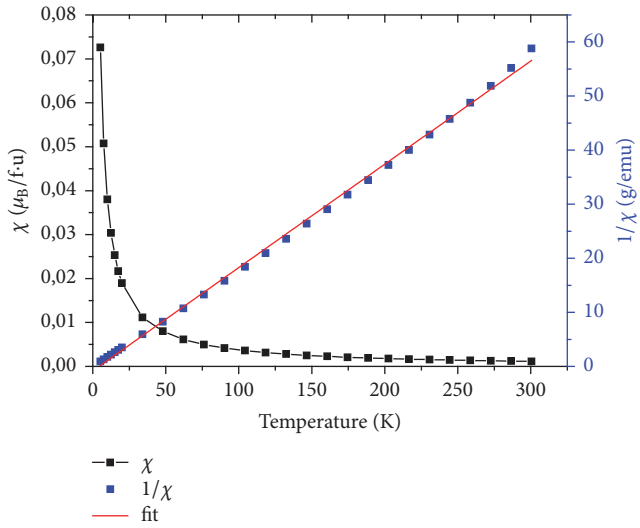

Figure 7: The magnetic susceptibility (χ) and inverse magnetic susceptibility ($1/\chi$) measurements as a function of temperature of $LiGd(PO_3)_4$.

can be explained by heavily distorted of PO_4 tetrahedra as are the GdO_8 polyhedra. We thus conclude that all compounds are stable at high temperatures and it is monophasic.

3.5. Magnetic Study. The magnetic susceptibility and inverse magnetic susceptibility versus temperature of $LiGd(PO_3)_4$, $LiGd_{0.98}Eu_{0.02}(PO_3)_4$, and $LiGd_{0.96}Eu_{0.04}(PO_3)_4$ are shown in Figures 7, 8, and 9, respectively. The only other reported type of rare earth polyphosphate structures are those of LGP: Eu^{3+}; and these were chosen because Gd^{3+} has an effective magnetic moment and the $4f^n$ electrons.

These curves prove that all three rare earth polyphosphate compounds exhibit a paramagnetic response. The nondoped LGP is the most paramagnetic one; this is explained by

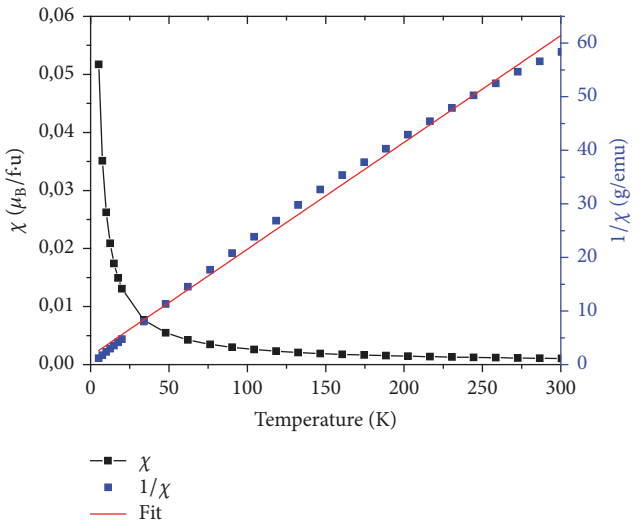

FIGURE 8: The magnetic susceptibility (χ) and inverse magnetic susceptibility ($1/\chi$) measurements as a function temperature of $LiGd_{0.98}Eu_{0.02}(PO_3)_4$.

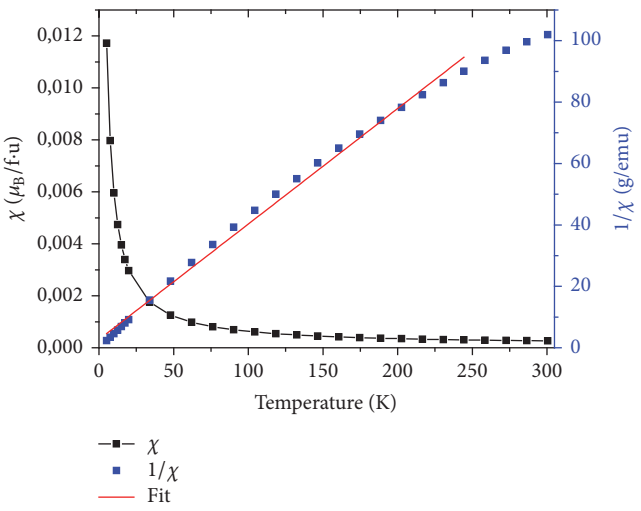

FIGURE 9: The magnetic susceptibility (χ) and inverse magnetic susceptibility ($1/\chi$) measurements as a function temperature of $LiGd_{0.96}Eu_{0.04}(PO_3)_4$.

their structural stability. Indeed, the addition of europium in the host disturbs samples in crystallinity. The response for LGP obeys Curie's Law very well; this is consistent with the ($^8S_{7/2}$) ground state of Gd^{3+}, which has no orbital angular momentum and so is unaffected by crystal field effects. Fitting, the temperature dependence of the inverse of susceptibility χ^{-1} in high temperatures is given by the formula [35]

$$\frac{1}{\chi} = \frac{(T - \theta_p)}{C} \tag{3}$$

TABLE 5: Values of C, μ_{eff}^{the} (μ_B), and μ_{eff}^{exp} (μ_B) for the $LiGd_{(1-x)}Eu_x(PO_3)_4$ (x=0, 0.02 and 0.04) compounds.

	x=0	x=0.02	x=0.04
C (μ_B.KT^{-1})	5.26	5	2.86
μ_{eff}^{the} (μ_B)	7.94	7.86	7.78
μ_{eff}^{exp} (μ_B)	6.50	6.32	4.65

where θ_P is the Weiss temperature and C is the Curie constant given by

$$C \approx \frac{\mu_0 N \mu_{eff}^2}{3K_B} \tag{4}$$

where N is the number of carriers of magnetic moment, μ_0 is the vacuum permeability, K_B is the Boltzmann constant, μ_B is the Bohr magnetron, and μ_{eff} is effective moment of carriers. Samples' structure consists of one magnetic species (i), possessing each a magnetic moment μ_{eff} (i); the magnetic susceptibility is given by the relation:

$$\chi = \mu_0 \frac{n_1 \mu_{eff}^2(1) + n_2 \mu_{eff}^2(2) + \cdots + n_i \mu_{eff}^2(i)}{3K_B T} \tag{5}$$

Generally, the magnetic moment is determined by

$$\mu_{eff} = g_J \sqrt{J(J+1)} \tag{6}$$

where g_J is the Lande factor and J is the total angular moment. The theoretical effective paramagnetic moment μ_{eff}^{the} for the samples can be calculated by

$$\mu_{eff}^{2\ the} = \left\{ x g_{Gd^{3+}}^2 J_{Gd^{3+}} \left(J_{Gd^{3+}} + 1 \right) \right\} \mu_B^2 \tag{7}$$

Curves of χ^{-1} versus temperature allow deducing μ_{eff}^{exp} values, which are summarized in Table 5. We can notice that the values of μ_{eff}^{the} decrease with the decrease of Gd percentage in the system, due to the important magnetic moment of Gd^{3+} ions (7.94μ_B). The comparison between the theoretical and the experimental effective moment values shows that the former are higher than the latter. This result can be associated with the increase of disorder in the matrix (LGP). On the other side, when the temperature increases to more than 75K, it induces a thermal agitation and causes magnetic moments disorientation of atoms in Eu doped LGP polyphosphates. Consequently, a decrease of paramagnetism is clearly observed (Figure 10).

3.6. Luminescence Properties

3.6.1. Excitation. Excitation spectra of $LiGd(PO_3)_4$, doped with europium (2, 4%) (Figure 11), are measured at 300K under emission with λ_{em}= 591 nm. Figure 11 shows broad band from 254 to 271 nm. These bands are assigned to the charge transfer bands (CTB), resulting from the transfer of an electron from the orbital $2p^6$ of the ligand O^{2-} to the empty

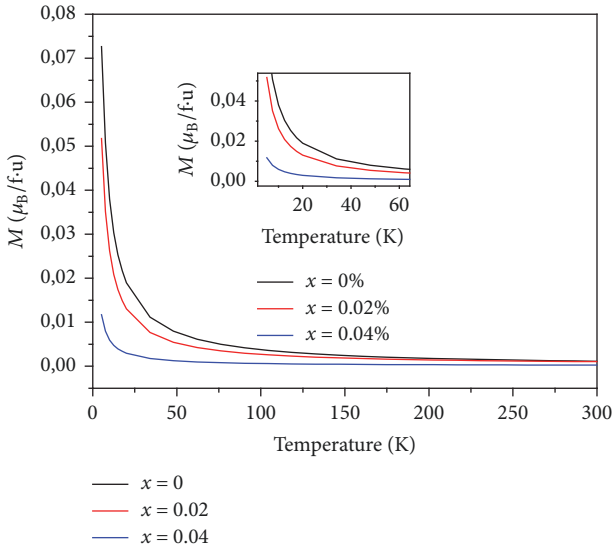

FIGURE 10: Magnetic measurements of $LiGd_{(1-x)}Eu_x(PO_3)_4$ (x=0, 0.02 and 0.04).

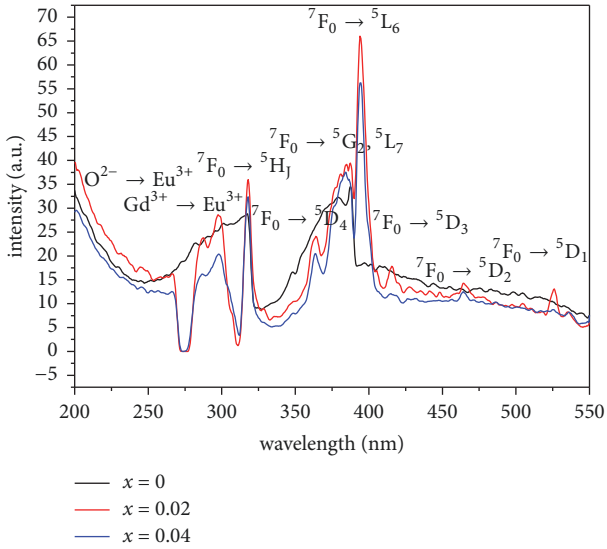

FIGURE 11: Excitation spectra with λ_{em}=591 nm of $LiGd_{(1-x)}Eu_x(PO_3)_4$ (x=0, 0.02 and 0.04) at 300 K.

state of the configuration [Xe]$4f^6$ of the Eu^{3+} ion (Eu^{3+}-O^{2-} transition). The maximum of the CTB is located at 245 nm. The differences between broadening and positions of the maxima intensities of the CTB in polyphosphate indicate their dependence on the host lattices [36]. This is due to the strong binding of the oxygen ligands in the polyphosphate compound [37].

At low frequencies, several groups of narrow bands in the spectral region 271-310 nm are clearly observed and assigned to $^8S_{7/2}\rightarrow{}^6H_J$, $^8S_{7/2}\rightarrow{}^6G_J$, $^8S_{7/2}\rightarrow{}^6D_J$, $^8S_{7/2}\rightarrow{}^6I_J$, and $^8S_{7/2}\rightarrow{}^6P_J$transitions of the Gd^{3+} ion. $LiYF_4$:Gd^{3+} crystal is used as reference to identify excitation bands, which describe the basis of the detailed energy level scheme proposed for

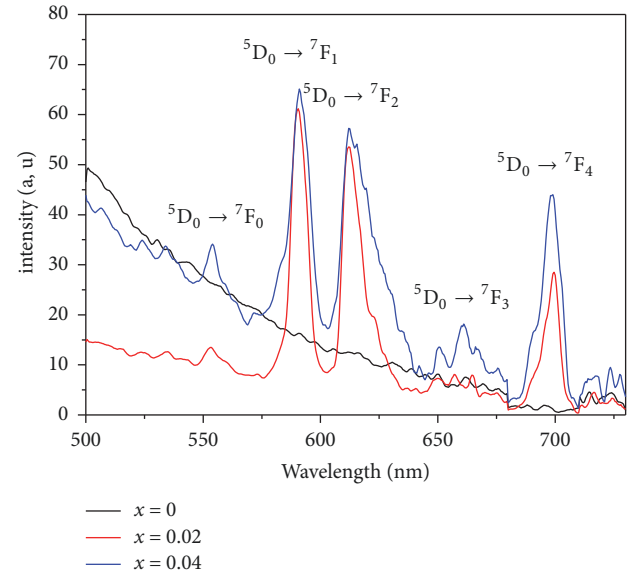

FIGURE 12: Emission spectra with λ_{ex}=394 nm of $LiGd_{(1-x)}Eu_x(PO_3)_4$ (x=0, 0.02 and 0.04) at 300 K.

the trivalent gadolinium [38]. The presence of band in the range between 271 and 310 nm indicates the presence of energy transfer between the two rare earths, which occurs from Gd^{3+} to Eu^{3+} in the matrix. However, there is no CTB of Eu^{3+}–O^{2-} or energy transfer band Gd^{3+}-Eu^{3+} above 310 nm. Excitation spectra within the wavelength range of 310–550 nm, show only the intrinsic transitions 4f-4f from the ground state $^7F_0$ to different excited levels (^5D, or ^5L) of Eu^{3+} ion. These transitions are assigned as follows: $^7F_0\rightarrow{}^5H_J$ at 316 nm, $^7F_0\rightarrow{}^5D_4$ at 362 nm, $^7F_0\rightarrow{}^5G_2$, $^5L_7$ at 382 nm, $^7F_0\rightarrow{}^5L_6$ at 393 nm, $^7F_0\rightarrow{}^5D_3$ at 417 nm, $^7F_0\rightarrow{}^5D_2$ at 464 nm,and $^7F_0\rightarrow{}^5D_1$ at 502 nm. All these assignments and wavelengths are given in Table 6. Most of the excitation bands are broadened and some of them overlap together to form a strong band, particularly the band between 369 and 409 nm with FWHM of about 18 nm.

The perfect match of this excitation band with the emission wavelength of NUV In GaN-based LED chips makes these phosphors conveniently useful in white LEDs [39]. Figure 11 shows that the band intensities increase with europium concentration. However, they maintain the same shape and position.

3.6.2. Emission. The emission spectra of condensed phosphates are recorded at ambient temperature (300K) and in the range of 500-750 nm after excitation with λ_{ex}= 394 nm (Figure 12). These spectra present the same shapes, with bands intensity proportional to Eu^{3+} active ion concentration. However, we notice that the undoped $LiGd(PO_3)_4$ polyphosphate does not emit light. The observed emission bands are attributed to the following transitions: $^5D_0\rightarrow{}^7F_J$ (where J = 0,1,2,3 or 4) of Eu^{3+} ion in the matrix $LiGd(PO_3)_4$ [40, 41].

Table 6: Excitation lines attribution of Eu^{3+} doped $LiGd(PO_3)_4$.

Wavelength (nm)	Attribution
287	$^7F_0 \rightarrow {}^5I_6$
294	$^7F_0 \rightarrow {}^5F_4$
297	$^7F_0 \rightarrow {}^5F_2$
6318	$^7F_0 \rightarrow {}^5H_6$
321	$^7F_0 \rightarrow {}^5H_4$
328	$^7F_0 \rightarrow {}^5H_7$
363	$^7F_0 \rightarrow {}^5D_4$
376	$^7F_1 \rightarrow {}^5D_4$
373-390	$^7F_0 \rightarrow {}^5G_{J(2,4)}$
394	$^7F_0 \rightarrow {}^5L_6$
405	$^7F_1 \rightarrow {}^5L_6$
416	$^7F_0 \rightarrow {}^5D_3$
464	$^7F_0 \rightarrow {}^5D_2$
526	$^7F_0 \rightarrow {}^5D_1$

Table 7: Emission attribution of Eu^{3+} doped $LiGd(PO_3)_4$.

Transitions	Wavelengths (nm)
$^5D_0 \rightarrow {}^7F_0$	554
$^5D_0 \rightarrow {}^7F_1$	578-601
$^5D_0 \rightarrow {}^7F_2$	604-634
$^5D_0 \rightarrow {}^7F_3$	660
$^5D_0 \rightarrow {}^7F_4$	686-706

Figure 12 proves the presence of five bands in the emission spectra where the most intense ones are those situated at 578-600 nm ($^5D_0 \rightarrow {}^7F_1$) and 604-634 nm ($^5D_0 \rightarrow {}^7F_2$). The other emission bands are observed at 554 nm ($^5D_0 \rightarrow {}^7F_0$), 660 nm ($^5D_0 \rightarrow {}^7F_3$), and 686-706 nm ($^5D_0 \rightarrow {}^7F_4$). The corresponding assignments and wavelengths of these emissions are given in Table 7. The relative intensities of the most intense transitions $^5D_0 \rightarrow {}^7F_0$, $^7F_1$, $^7F_2$ $^7F_3$ and $^7F_4$ are strongly influenced by the nature of the host and the crystalline environment [42]. Therefore, the dominance of magnetic dipole (MD) transition $^5D_0 \rightarrow {}^7F_1$ of Eu^{3+} means that Eu^{3+} occupies a site in the crystal lattice with inversion symmetry. However, in the case of absence of symmetry inversion in the site of Eu^{3+}, the main emission would be the electric dipole (ED) transition $^5D_0 \rightarrow {}^7F_2$ [43]. The synthesized polyphosphates showed that orange emission transition ($^5D_0 \rightarrow {}^7F_1$) is slightly dominated. This indicates that Eu^{3+} occupies a site in the crystal lattice with symmetry inversion.

4. Conclusion

Polyphosphates of rare earth and alkali metal LGP:Eu^{3+} were successfully synthesized by solid-state reaction at 730°C. XRD patterns proved that the obtained samples crystallize in a monoclinic single phase with space group I 2/a and following cell parameters a= 9.635(3) Å, b= 7.035(3) Å, c= 13.191(3) Å, β= 90.082°, V= 894.214 Å^3, and Z= 4. The synthesized polyphosphates showed a good thermal stability until 940°C. Spectroscopic analyses by IR and Raman spectra confirmed the acyclic zig-zag chain of $(PO_4)^{3-}$ in LGP structure, involving GdO_8 dodecahedra and LiO_4 polyhedra. The magnetic susceptibility carried out on single crystals revealed that the title compounds were paramagnetic between 5 and 300 K. An increase in excitation and emission bands intensities was observed with the increase of europium concentration. The presence of band in the range between 271 and 310 nm in excitation spectra proved the energy transfer process from Gd^{3+} to Eu^{3+}. The dominance of $^5D_0 \rightarrow {}^7F_1$ transition in the emission spectra confirms that Eu^{3+} occupies a site in the crystal lattice with symmetry inversion. The change in transition bands intensity proves that LGP phosphates affect europium environment.

Conflicts of Interest

There are no conflicts of interest regarding the publication of this paper.

References

[1] L. Campayo, F. Audubert, and D. Bernache-Assollant, "Synthesis study of alkaline-bearing rare earth phosphates with rhabdophane structure," *Solid State Ionics*, vol. 176, no. 35-36, pp. 2663–2669, 2005.

[2] J. Zhu, H. Chen, Y. Wang, H. Guan, and X. Xiao, "Structure determination, electronic and optical properties of rubidium holmium polyphosphate $RbHo(PO_3)_4$," *Journal of Molecular Structure*, vol. 1030, pp. 204–208, 2012.

[3] S. Yang and Z. Chen, "The Study on Aging and Degradation Mechanism of Ammonium Polyphosphate in Artificial Accelerated Aging," *Procedia Engineering*, vol. 211, pp. 906–910, 2018.

[4] M. El Masloumi, I. Imaz, J. P. Chaminade et al., "Synthesis, crystal structure and vibrational spectra characterization of $MILa(PO_3)_4$ (MI = Na, Ag)," *Journal of Solid State Chemistry*, vol. 178, pp. 3581–3588, 2005.

[5] J. M. Cole, M. R. Lees, J. A. K. Howard, R. J. Newport, G. A. Saunders, and E. Schönherr, "Crystal Structures and Magnetic Properties of Rare-Earth Ultraphosphates, RP_5O_{14} (R=La, Nd, Sm, Eu, Gd)," *Journal of Solid State Chemistry*, vol. 150, pp. 377–382, 2000.

[6] J. J. Gavaldà, I. Parreu, R. Solé, X. Solans, F. Díaz, and M. Aguiló, "Growth and Structural Characterization of $Rb_3Yb_2(PO_4)_3$: A New Material for Laser and Nonlinear Optical Applications," *J. Chemistry of Materials*, vol. 17, no. 26, pp. 6746–6754, 2005.

[7] M. Ferid and K. Horchani-Naifer, "Structure and ionic conductivity of $NaCeP_2O_7$," *Journal of Solid State Ionics*, vol. 176, pp. 1949–1953, 2005.

[8] K. Jaouadi, N. Zouari, T. Mhiri, and M. Pierrot, "Synthesis and crystal structure of sodium–bismuth polyphosphate $NaBi(PO_3)_4$," *Journal of Crystal Growth*, vol. 273, no. 3-4, pp. 638–645, 2005.

[9] M. Amria, N. Zouaria, T. Mhiri, A. Daoud, and P. Gravereau, "Crystal structure and conductivity investigation of $KDyP_4O_{12}$: a new potassium dysprosium cyclotetraphosphate," *Journal of Molecular Structure*, vol. 782, pp. 16–23, 2006.

[10] D. P. Minh, A. R. Sane, N. Semlal, P. Sharrock, and A. Nzihou, "Alkali polyphosphates as new potential materials for thermal

energy storage," *Journal of Solar Energy*, vol. 157, pp. 277–283, 2017.

[11] Z. Mua, Y. Hub, L. Chen et al., "A reddish orange stoichiometric phosphor $LiEu(PO_3)_4$ for white light-emitting diodes," *Journal of Ceramics International*, vol. 40, pp. 2575–2579, 2014.

[12] J. Zhong, H. Liang, Q. Su, J. Zhou, I. V. Khodyuk, and P. Dorenbos, "Radioluminescence properties of Ce^{3+}-activated $MGd(PO_3)_4$ (M = Li, Na, K, Cs)," *Optical Materials*, vol. 32, no. 2, pp. 378–381, 2009.

[13] J. Gu, J. Zhong, H. Liang, J. Zhang, and Q. Su, "Competitive absorption of Eu^{3+} and Tb^{3+}codoped in $NaGd(PO_3)_4$ phosphors," *Chemical Physics Letters*, vol. 592, pp. 261–264, 2014.

[14] B. Han, H. Liang, H. Ni et al., "Intense red light emission of Eu^{3+}-doped $LiGd(PO_3)_4$ for mercury-free lamps and plasma display panels application," *J. of Optics Express*, vol. 17, pp. 7138–7144, 2009.

[15] T. Shalapska, G. Stryganyuk, P. Demchenko, A. Voloshinovskii, and P. Dorenbos, "Luminescence properties of Ce^{3+}-doped $LiGdP_4O_{12}$ upon vacuum-ultraviolet and x-ray excitation," *Journal of Physics: Condensed Matter*, vol. 21, no. 44, Article ID 445901, 2009.

[16] B. Han, H. Liang, Y. Huang, Y. Tao, and Q. Su, "Vacuum Ultraviolet–Visible Spectroscopic Properties of Tb^{3+} in $Li(Y, Gd)(PO_3)_4$: Tunable Emission, Quantum Cutting, and Energy Transfer," *The Journal of Physical Chemistry*, vol. C114, no. 14, pp. 6770–6777, 2010.

[17] R. Shi, G. Liu, H. Liang, Y. Huang, Y. Tao, and J. Zhang, "Consequences of ET and MMCT on Luminescence of Ce^{3+}, Eu^{3+}, and Tb^{3+}-doped $LiYSiO_4$," *Inorganic Chemistry*, vol. 55, no. 15, pp. 7777–7786, 2016.

[18] A. Krasnikov, T. Shalapska, G. Stryganyuk, A. Voloshinovskii, and S. Zazubovich, "Photoluminescence and energy transfer in Eu^{3+}-doped alkali gadolinium phosphates," *Physica Status Solidi (b) – Basic Solid State Physics*, vol. 250, no. 7, pp. 1418–1425, 2013.

[19] J. Zhong, H. Liang, Q. Su, and J. Zhou, "Luminescence properties of $NaGd(PO_3)_4$:Eu^{3+} and energy transfer from Gd^{3+} to Eu^{3+}," *Applied Physics B: Lasers and Optics*, vol. 98, pp. 139–147, 2010.

[20] W. Xu, J.-G. Dai, Z. Ding, and Y. Wang, "Polyphosphate-modified calcium aluminate cement under normal and elevated temperatures: Phase evolution, microstructure, and mechanical properties," *Ceramics International*, vol. 43, no. 17, pp. 15525–15536, 2017.

[21] B. Liu, Y. Chen, C. Shi, H. Tang, and Y. Tao, "Visible quantum cutting in BaF_2: Gd, Eu downconversion," *Journal of Luminescence*, vol. 101, no. 1-2, pp. 155–159, 2003.

[22] H. Kondo, T. Hirai, and S. Hashimoto, "Dynamical behavior of quantum cutting in alkali gadolinium fluoride phosphors," *Journal of Luminescence*, vol. 108, no. 1-4, pp. 59–63, 2004.

[23] N. Kodama and Y. Watanabe, "Visible quantum cutting through downconversion in Eu^{3+}-doped KGd_3F_{10} and KGd_2F_7 crystals," *Applied Physics Letters*, vol. 84, no. 21, pp. 4141–4143, 2004.

[24] P. Ghosh, S. Tang, and A.-V. Mudring, "Efficient quantum cutting in hexagonal $NaGdF_4$:Eu^{3+}nanorods," *Journal of Materials Chemistry*, vol. 21, no. 24, pp. 8640–8644, 2011.

[25] J. Legendziewicz, M. Guzik, and J. Cybińska, "VUV spectroscopy of double phosphates doped with rare earth ions," *Optical Materials*, vol. 31, no. 3, pp. 567–574, 2009.

[26] S. Hammami, S. Sebai, D. Jegouso, V. Reita, N. C. Boudjada, and A. Megriche, "Magnetic and Photon Cascade Emission of Gd^{3+} of $NaGd(PO_3)_4$ Monocrystal Under Appropriate Synthesis Conditions," *Journal of Physical Chemistry & J Biophysics*, vol. 7, pp. 2161-0398, 2017.

[27] H. Ettis, H. Naïli, and T. Mhiri, "The crystal structure, thermal behaviour and ionic conductivity of a novel lithium gadolinium polyphosphate $LiGd(PO_3)_4$," *Journal of Solid State Chemistry*, vol. 179, no. 10, pp. 3107–3113, 2006.

[28] R. Shannon, "Revised effective ionic radii and systematic studies of interatomic distances in halides and chalcogenides," *Acta Crystallographica Section A: Foundations of Crystallography*, vol. 32, pp. 751–767, 1976.

[29] T. Gholami and M. Salavati-Niasari, "Green facile thermal decomposition synthesis, characterization and electrochemical hydrogen storage characteristics of $ZnAl_2O_4$nanostructure," *International Journal of Hydrogen Energy*, vol. 42, no. 27, pp. 17167–17177, 2017.

[30] S. Sebai, S. Hammami, A. Megriche, D. Zambon, and R. Mahiou, "Synthesis, structural characterization and VUV excited luminescence properties of $Li_xNa_{(1-x)}Sm(PO_3)_4$polyphosphates," *Optical Materials*, vol. 62, pp. 578–583, 2016.

[31] T. Sun, Y. Zhang, P. Shan et al., "Growth, structure, thermal properties and spectroscopic characteristics of Nd^{3+}- doped $KGdP_4O_{12}$ crystal," *PLoS ONE*, vol. 9, no. 6, Article ID e100922, 2014.

[32] W. Rekik, H. Naïli, T. Mhiri, and T. Bataille, "$[NH_3(CH_2)_2NH_3][Co(SO_4)_2(H_2O)_4]$: Chemical preparation, crystal structure, thermal decomposition and magnetic properties," *Materials Research Bulletin*, vol. 43, no. 10, pp. 2709–2718, 2008.

[33] J. Zhang, Z. Zhang, W. Zhang et al., "Polymorphism of $BaTeMo_2O_9$: a new polar polymorph and the phase transformation," *Chemistry of Materials*, vol. 23, no. 16, pp. 3752–3761, 2011.

[34] K. Jaouadi, H. Naili, N. Zouari, T. Mhiri, and A. Daoud, "Synthesis and crystal structure of a new form of potassium–bismuth polyphosphate $KBi(PO_3)_4$," *Alloys Compds*, vol. 354, no. 30, p. 104, 2003.

[35] D. Petrov, B. Angelov, and V. Lovchinov, "Magnetic and XPS studies of lithium lanthanide tetraphosphates $LiLnP_4O_{12}$ (Ln=Nd, Gd, Er)," *Journal of Rare Earths*, vol. 31, no. 5, pp. 485–489, 2013.

[36] S. Hachani, B. Moine, A. El-akrmi, and M. Férid, "Luminescent properties of some ortho- and pentaphosphates doped with Gd^{3+}–Eu^{3+}: Potential phosphors for vacuum ultraviolet excitation," *Optical Materials*, vol. 31, no. 4, pp. 678–684, 2009.

[37] M. Ferhi, K. Horchani-Naifer, and M. Férid, "Spectroscopic properties of Eu^{3+}-doped $KLa(PO_3)_4$ and $LiLa(PO_3)_4$ powders," *Optical Materials*, vol. 34, no. 1, pp. 12–18, 2011.

[38] R. T. Wegh, H. Donker, A. Meijerink, R. J. Lamminmäki, and J. Hölsä, "Vacuum-ultraviolet spectroscopy and quantum cutting for Gd^{3+} in $LiYF_4$," *Physical Review B*, vol. 56, no. 21, pp. 13841–13848, 1997.

[39] M. Abdelhedi, K. Horchani-Naifer, M. Dammak, and M. Ferid, "Structural and spectroscopic properties of pure and doped $LiCe(PO_3)_4$," *Materials Research Bulletin*, vol. 70, pp. 303–308, 2015.

[40] E. E. S. Teotonio, H. F. Brito, M. C. F. C. Felinto, L. C. Thompson, V. G. Young, and O. L. Malta, "Preparation, crystal structure and optical spectroscopy of the rare earth complexes (RE^{3+}=Sm, Eu, Gd and Tb) with 2-thiopheneacetate anion," *Journal of Molecular Structure*, vol. 751, no. 1-3, pp. 85–94, 2005.

[41] A. Mbarek, "Synthesis, structural and optical properties of Eu^{3+}-doped $ALnP_2O_7$(A = Cs, Rb, Tl; Ln = Y, Lu, Tm) pyrophosphates phosphors for solid-state lighting," *Journal of Molecular Structure*, vol. 1138, pp. 149–154, 2017.

[42] D. C. Tuan, R. Olazcuaga, F. Guillen, A. Garcia, B. Moine, and C. Fouassier, "Luminescent properties of Eu^{3+}-doped yttrium or gadolinium phosphates," *J. of Physics*, vol. 123, pp. 259–263, 2005.

[43] M. Gaft, G. Panczer, R. Reisfeld, I. Shinno, B. Champagnon, and G. Boulon, "Laser-induced Eu^{3+} luminescence in zircon $ZrSiO_4$," *Journal of Luminescence*, vol. 87, pp. 1032–1035, 2000.